Effects of Saturated and Dry Land Surfaces on the Tropical Circulation and Precipitation in a General Circulation Model

KERRY H. COOK*

GFDL/NOAA, Princeton University, Princeton, New Jersey

ANAND GNANADESIKAN**

Department of Physics, Princeton University, Princeton, New Jersey

(Manuscript received 14 February 1990, in final form 25 October 1990)

ABSTRACT

A comprehensive rhomboidal-15 general circulation model with idealized boundary conditions is used to investigate the effects of interactions between the tropical circulation and continental climate on the precipitation distribution. Sea surface temperatures are fixed and zonally uniform and, along with the solar forcing, establish perpetual solstice conditions. Clouds are also prescribed and zonally uniform. Experiments with dry and saturated land surfaces are compared with an all-ocean control integration.

The winter hemisphere of the saturated continent is cooler than the prescribed ocean surface at the same latitude, and the summer hemisphere is warmer. When the surface is dry, the maximum summer hemisphere warming is four times larger than in the saturated surface case and extends into the winter hemisphere. The ITCZ is shifted farther into the summer hemisphere and enhanced near the coasts over the saturated continent, but it is interrupted in crossing the dry surface.

The modification of the precipitation distribution over the saturated land surface can be understood by considering the low-level flow. Over the dry surface, however, low-level horizontal moisture convergence and precipitation patterns are unrelated. The extreme dryness of the surface and the atmosphere below 830 mb eliminates condensation in the lower troposphere despite the increased instability of the tropical atmosphere. Condensation in the middle troposphere also decreases over the western half of the continent.

1. Introduction

Interactions between land surfaces and the atmosphere are receiving increased attention from the climate modeling community. Understanding how the presence and characteristics of land surfaces influence the state of the atmosphere and are, in turn, affected by the atmosphere is crucial to understanding the climate and how it changes.

Models incorporating complex surface processes, including physically based descriptions of soils and vegetation, have been developed over the last decade (e.g., Dickinson 1984; Sellers et al. 1986). When these models are coupled to general circulation models (GCMs) significant differences are reported due to land surface/atmosphere interactions, especially in connection with variations in climate statistics on time scales ranging from days to several weeks. The relative importance of these processes in GCMs is less clear at longer time scales and in the maintenance of an equilibrium climate. The difficulty of quantifying the relevance of these processes is compounded by a shortage of observations near the surface and the small horizontal space scales that are related to the distribution of land surface characteristics.

In this study we take an idealized approach to understanding the role that land surface/atmosphere interactions play in establishing features of the climate by using a GCM with simplified boundary conditions. We concentrate on the tropics and subtropics and ask how the large-scale atmospheric circulation is related to land surface conditions, and how the continental climate is established in relation to this circulation. The atmospheric model is the comprehensive GCM developed by the Climate Dynamics Group at NOAA's Geophysical Fluid Dynamics Laboratory (GFDL), but the boundary conditions of the model are kept as simple as possible to isolate processes involved in the mutual adjustment of the continental climate and the tropical circulation.

Models of the atmosphere that are less comprehensive than a GCM have been used to study the response of the tropical circulation to a given diabatic heating.

* Present affiliation: Department of Soil, Crop and Atmosphere Sciences, Cornell University, Ithaca, New York.

** Present affiliation: MIT/WHOI Joint Program in Physical Oceanography, Cambridge, Massachusetts.

Corresponding author address: Dr. Kerry H. Cook, 1113 Bradfield Hall, Cornell University, Ithaca, NY 14853.

Gill-Matsuno models have been particularly useful for studying the connection between tropical heating (especially due to sea surface temperature anomalies) and the low-level wind field (e.g., Gill 1980). These models effectively assume that the diabatic and adiabatic heating balance throughout the tropical troposphere and suggest relevant dynamical frameworks for studying how the tropical circulation adjusts to modifications of the diabatic heating field.

GCMs are used to study the effects of feedback between the atmosphere and land surface, including interactive atmospheric dynamics and hydrological cycle. Sud and Fennessy (1984) describe experiments with a 9-layer GCM with $4° \times 5°$ horizontal resolution. With 16 days of "spinup" from realistic June initial conditions, they compared an interactive soil moisture simulation with a simulation in which the Sahel, Thar Desert, North American Great Plains, and northeast Brazil were forced to remain dry. The dry surface conditions resulted in a slight increase in precipitation over the Sahel and the Great Plains due to increased low-level moisture convergence. Precipitation increased significantly over the Thar Desert due to an enhanced monsoonal circulation and decreased over Brazil. Rind (1982), on the other hand, simulates drying due to reduced soil moisture in North America during summer with three integrations of an 8° and 10° GCM. An earlier study with a limited-area tropical model by Walker and Rowntree (1977) also found less precipitation over dry surfaces. Shulka and Mintz (1982) compared the climate of a GCM with evapotranspiration at the potential rate over dry surfaces in the interiors of large continents. Surface drying had little effect on precipitation rates in southeast Asia and India in their experiments.

The purpose of these experiments is to examine the tropical and subtropical atmospheric response to a drying of the surface in an equilibrium state, i.e., giving the atmosphere as much time as it needs to adjust to the surface conditions. The results are applicable to interannual time scales, and not seasonal time scales. The experiments are designed to allow us to focus on certain mechanisms and exclude other influences. The disadvantage of this approach is that the importance of a particular reaction by the climate system can be artificially magnified or altered in unpredictable ways since possibly competing or ameliorating processes are excluded. However, once the basic response is established, complexity can be added in subsequent studies.

The model used in this investigation and the experiments conducted are described in section 2, and the model atmosphere is compared with observations for the control integration. The model is compared with observed features in section 3. The continental climates are discussed in section 4, and section 5 is concerned with modifications of the tropical circulation. Section 6 summarizes the results and conclusions.

2. Model and experiments

a. Model description

The model used in this series of experiments is a version of the GCM developed by the Climate Dynamics Group of NOAA's Geophysical Fluid Dynamics Laboratory. The model solves the primitive equations plus a prognostic equation for water vapor mixing ratio using the semispectral technique described in Gordon and Stern (1980). The rhomboidal-15 truncation of the spectral components is equivalent to a horizontal grid resolution of approximately 4.5° latitude and 7.5° longitude. The governing equations are solved on nine vertical levels in sigma coordinates.

In these experiments the model's boundary conditions are highly idealized. The purpose of the idealization is to remove zonal asymmetries and differences between the hemispheres that are due to processes not directly related to the presence of a continent. Cloud height, thickness, and fractional cover are not predicted, but held fixed in each hemisphere at the zonally averaged values observed by London (1957) for the Northern Hemisphere. Ozone concentrations are also zonally uniform and the same in both hemispheres. Sea ice is not allowed to form, and the surface is flat.

The only differences between the hemispheres are the latitudinal variations of the solar radiation and the sea surface temperature (SST). The model is run in a "perpetual season" mode, so that the day length and the sun's zenith angle represent solstice conditions. Diurnal variation is not included so the incoming solar radiation is the same at a given point every time step. The perpetual solar forcing results in a stable and reasonable climate state when sea surface temperatures are also prescribed. The zonally symmetric SST, T^*, is given by

$$T^* = 287 - 10 \sin(\theta) - (0.3)(40)[3 \sin^2(\theta) - 1], \quad (1)$$

where θ is latitude. This SST prescription results in a lower boundary condition similar to an average solstice SST distribution (Fig. 1). The temperature maximum of 301 K is at about 7° in the summer hemisphere, and the polar temperatures differ by 20 K with 250 K near the winter pole and 270 K near the summer pole.

The treatment of the land surface heat balance and hydrology, and the convective adjustment parameterization, are of particular relevance for this study and are described in more detail.

1) LAND SURFACE HEAT BALANCE

Over land, T^* is the "ground temperature" and it is allowed to change in response to the surface heat balance equation

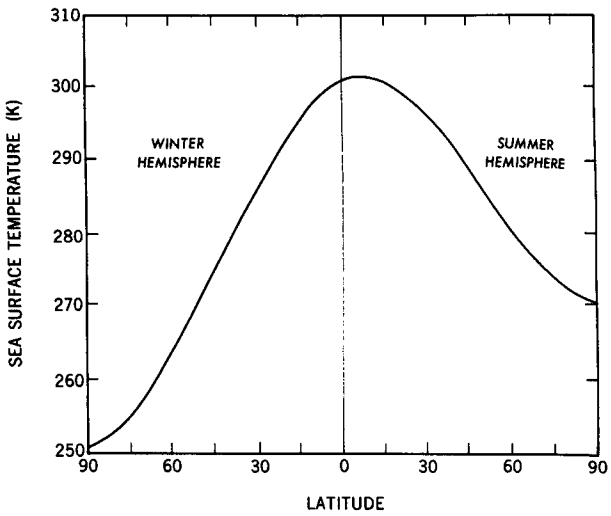

FIG. 1. Prescribed sea surface temperatures from the control integration.

$$\partial T^*/\partial t = R + S + \mathrm{SH} + \mathrm{LH} + M, \qquad (2)$$

where R is the net downward longwave flux at the surface, S is the solar flux absorbed at the ground, SH is the sensible heat flux (defined positive when the ground is heated), LH is the latent heat flux (negative when evaporation cools the surface), and M accounts for energy taken in melting snow. Over the fixed SST oceans, if the right-hand side of (2) does not sum to zero there is a net heat loss from, or gain to, the model climate system. Over the land surface, on the other hand, T^* changes every time step in response to the atmospheric conditions reflected in the surface heat budget components.

The terms of the heat budget depend on surface and atmospheric conditions. The sensible heat flux is

$$\mathrm{SH} = \rho c_p C_D |\mathbf{V}_9| (T_9 - T^*), \qquad (3)$$

where ρ is the density of the surface air, C_D is a drag coefficient, $|\mathbf{V}_9|$ is the magnitude of the wind in the lowest model layer, and T_9 is the temperature in the lowest model layer. The drag coefficient is a parameterization of surface roughness—if the surface is rougher, C_D is larger and the exchange of sensible heat between the ground and the surface air is enhanced. Values commonly used are $C_D = 0.001$ for oceans and $C_D = 0.003$ for land. In these experiments, $C_D = 0.001$ everywhere.

The latent heat flux is calculated according to

$$\mathrm{LH} = L f(w/w_{\mathrm{FC}}) E_p \qquad (4)$$

where L is the latent heat of vaporization and E_p is the potential evaporation given by

$$E_p = \rho C_D |\mathbf{V}_9| (q_9 - q_{T^*}), \qquad (5)$$

where q_9 is the mixing ratio at the lowest model level and $q_s(T^*)$ is the saturation mixing ratio at temperature T^*. The function $f(w/w_{\mathrm{FC}})$ in (4) accounts for the dependence of the evaporation on the soil moisture, w. Its value is 1 if $w > 11.25$, but it inhibits evaporation for drier conditions, i.e.,

$$f(w/w_{\mathrm{FC}}) = w/(0.75 w_{\mathrm{FC}}) \quad \text{if} \quad w < 11.25. \qquad (6)$$

The budget for water in the soil is computed using the so-called "bucket method." All land surfaces are assigned a soil moisture field capacity (w_{FC}) of 15 cm of water. If the net results of evaporation and precipitation bring the soil moisture above this value, the excess water is assumed to run off and is no longer accounted for in the hydrological budget. Delworth and Manabe (1988) include a complete description of this parameter and the role of the potential evaporation in the heat and water budgets.

The radiative components of the surface heat balance are the shortwave and longwave fluxes,

$$S = (1 - \alpha) S_i \qquad (7)$$

and

$$R = \sigma T^{*4} - R_b, \qquad (8)$$

where α is the surface albedo, S_i is the incident solar radiation, σ is the Stefan-Boltzmann constant, and R_b is the longwave back radiation from the atmosphere to the ground. Here R_b is the downward reemission of the outgoing terrestrial radiation by greenhouse gasses and changes due to temperature changes and the redistribution of water molecules in the atmosphere since the CO_2 concentration is fixed.

2) CONDENSATION AND PRECIPITATION

The amount of precipitation predicted by the model in a given time step is equal to the amount of water vapor that condenses in the atmospheric column. No mechanism for reevaporation of condensed water is included when, for example, a raindrop travels through a dry layer below its level of condensation. Condensation is simulated whenever the air is supersaturated. If air is supersaturated and the moist adiabatic lapse rate is exceeded, the adjustment is done differently than for supersaturation alone. In the real atmosphere, the occurrence of excessive moist lapse rates and supersaturation are often related, and nature makes adjustments back to stability and 100% relative humidity on a time and space continuum not possible in a model. To approximate this adjustment, the following steps are performed in the GCM after the temperature tendency has been calculated according to the governing equations and temperatures have been adjusted iteratively so that the dry adiabatic lapse rate is not exceeded between any two layers:

(i) Calculate moist adiabatic lapse rate between each layer using layer tempertures and a look up table for saturation vapor pressure. Compare with computed lapse rate and mark locations with excessive lapse rates and supersaturated air.

(ii) Compare the computed and saturation mixing ratios everywhere, marking supersaturated locations.

(iii) In adjacent layers between which the moist adiabatic lapse rate is exceeded and within which the air is supersaturated, calculate a temperature change (δT_a) and a condensate amount (P_a) such that the final temperature and mixing ratio satisfy the saturated moist adiabatic lapse rate equation, the layers are saturated, and energy is conserved. (This can be performed over blocks of more than two layers.)

(iv) In regions that were found supersaturated in (2), *but not adjusted in step* 3, condense enough water vapor to bring the layer back to supersaturation (P_c) based on the dry—but not moist—adiabatically adjusted layer temperature; calculate the temperature change $\delta T_c = LP_c$.

(v) Calculate the new layer temperatures, $T_{new} = T + \delta T_c + \delta T_a$, and the total precipitation, $P = P_c + P_a$.

Note that with this method for calculating precipitation, it is not really very meaningful to distinguish between precipitation due to the convective adjustment and precipitation due to an individual layer being supersaturated.

The idealized GCM, with the entire surface covered by the prescribed temperature ocean, reproduces a reasonable vertical and latitudinal structure for the atmospheric winds and temperatures. Figure 2a shows the zonal-mean zonal wind from a 700-day integration of the model. The difference between the hemispheres is evident, with generally stronger mean winds at all levels in the winter hemisphere. Low-level easterlies up to 6 m s^{-1} occur in the winter hemisphere tropics. This is similar to the observations, except that easterlies are not maintained throughout the full depth of the troposphere in the model. Westerlies prevail in the middle latitudes of both hemispheres, reaching 8 m s^{-1} at the surface in the winter hemisphere. The westerly wind maxima are at nearly the same latitudes in both hemispheres, while the observed winter maximum is 10°–15° closer to the equator than the summer hemisphere maximum. The winter westerly maximum is also some 10 m s^{-1} stronger than the average observed values. This is probably related to the lack of zonal asymmetries (especially the lack of topography) in the boundary conditions.

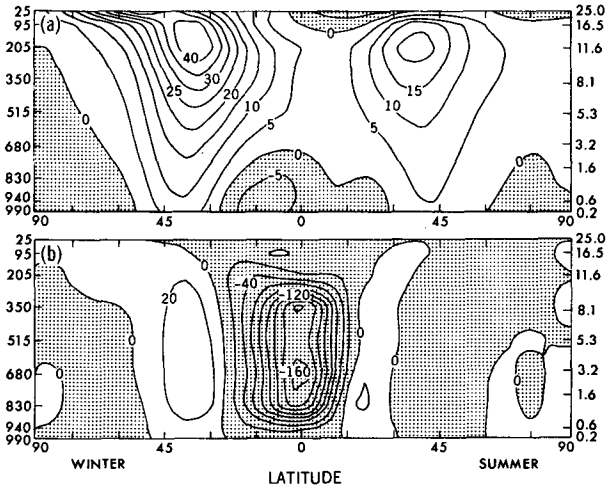

FIG. 2. (a) Zonal-mean zonal wind from the control integration. Contours are 5 m s^{-1}. (b) Meridional streamfunction from CTL with 20 × 10^9 kg s^{-1} contours.

Figure 2b is the two-dimensional streamfunction

$$\psi = [2\pi a \cos(\theta)]/g \int_p^{p_o} \bar{v}\, dp, \qquad (9)$$

where a is the radius of the earth, g is the acceleration of gravity, p_0 is surface pressure, and $\bar{v}$ is the zonally averaged meridional wind speed. Thermally direct (Hadley) circulations cover tropical and polar latitudes in the model as in the observed mean meridional circulation. The stronger Hadley cell that extends from 15° in the summer hemisphere to 20° in the winter hemisphere is slightly weaker than the observed mass flux (e.g., Newell et al. 1972). It is also centered more squarely on the equator than the observed cell, which is near 10° latitude in the winter hemisphere. The summer hemisphere direct cell in the model is also slightly weaker than observed, and the difference in their locations in each hemisphere is not as pronounced as in the observations.

The zonal-mean climate of the control integration compares well with observations, especially when the idealized nature of the model formulation is considered, and provides a good control climatology for the experiments with idealized continents.

b. Experiments

Experiments are performed in which the surface boundary conditions are modified to include a large tropical continent. The continent is centered at the equator and extends 45° of latitude into each hemisphere; it is 60° wide in longitude. In the model's grid point space projection, the continent is 8 grid points wide in longitude and covers 20 north–south grid points. Two experiments are discussed. In one, the continental surface hydrology is active, so that the land surface can respond to changes in the hydrological cycle and also change temperature in response to the surface heat balance. Snow can accumulate on the continent, but the snow-free land albedo and surface roughness (expressed as a drag coefficient) are the same as for the

ocean surface ($\alpha = 0.1$, $C_D = 0.001$). The other experiment is identical except that the continental surface hydrology is not active; the soil layer is prescribed saturated at all times, regardless of changes in the atmospheric hydrological cycle. This type of surface boundary condition has been called a "swamp" since it is like a surface covered by a thin but inexhaustible layer of water.

The experiments are each 700 days long, with 200 days devoted to spinup from an isothermal, motionless atmosphere with a saturated land surface and 50% relative humidity. The climate statistics from the last 500 days of the integration are averaged to form climatologies. Although we have not conducted rigorous statistical significance tests of the results, we estimate the spatial variability of atmospheric fields away from the continents and compare them with the magnitudes of the signals. Also, applicable to the case of dry continent, a similar experiment was integrated for a total of 1000 days, and the two 500-day mean climates were found to be in close agreement. This suggests that 500 days is sufficient time to establish the equilibrium between the land surface and the circulation.

The results of the experiments are presented and analyzed in the following section. The winter hemisphere is at the top in the figures so that Northern (Southern) Hemisphere readers who like their own hemisphere at the top of figures may think of the simulation as a perpetual January (July).

3. Comparison with observations

The purpose of a comparison with observations is to identify gross features of climate that are associated with the presence of large continents in the tropics and subtropics. Detailed agreement is not expected, of course, because of the idealized nature of the experiments. For example, the model continent is flat, but topography plays an important role in establishing continental climates in many regions.

Figure 3a is the climatological temperature for the lowest model layer ($\sigma = 0.99$) over the dry continent.

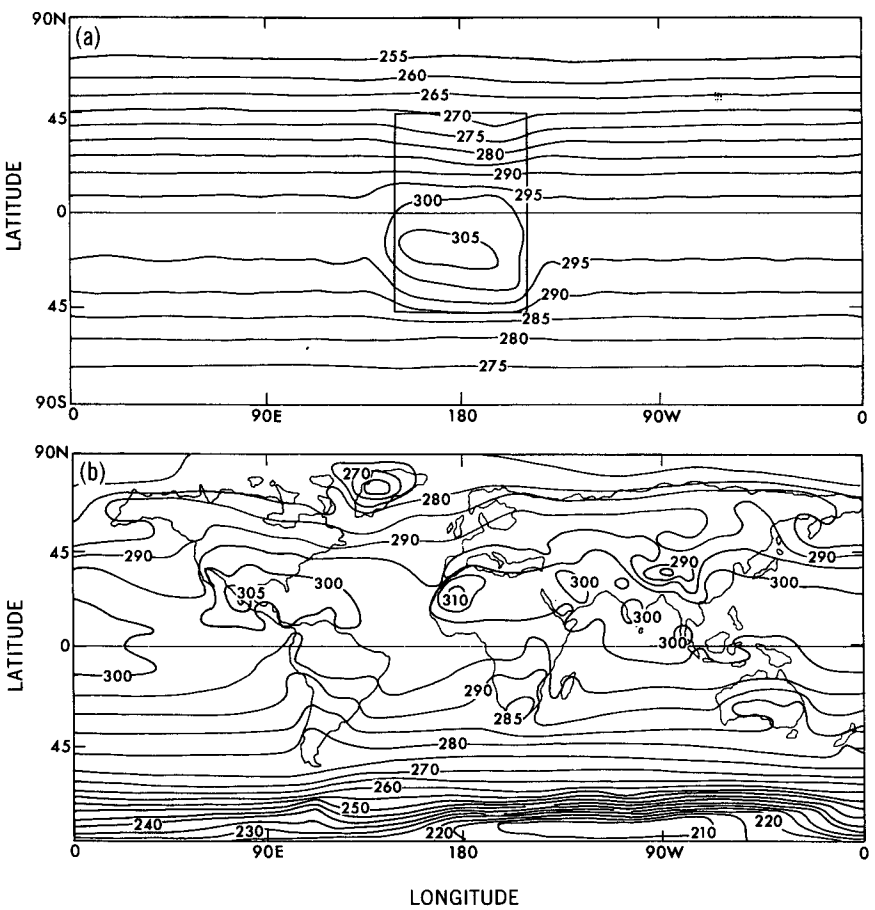

FIG. 3. Surface air temperatures distributions for (a) GCM with hydrologically active (dry) continent; (b) observed JJA (Dickinson 1986). Contour intervals are 5 K.

Summer temperatures in the continental interior are warmer than the surrounding marine air, with maximum differences up to 10 K near the subsolar latitude. In the winter hemisphere the land surface is up to 5 K cooler, with the maximum effect at the highest continental latitude.

The model's summer hemisphere temperatures are similar to temperatures over the northern half of Africa averaged over June, July, and August (JJA) (Fig. 3b from Dickinson 1986) and the model's winter hemisphere to northern Africa in December, January, and February (DJF) (not shown). Surface air temperatures near the center of the idealized continent reach 307 K in the summer hemisphere, and the interior of northern Africa between 300 K and 305 K over a large area during JJA, and over 310 K in the west. During DJF, low-level air temperatures over northern Africa are approximately 5 K cooler than the low-level marine air. The effect of differences in heat capacity between the ocean and the land is one factor responsible for the land–sea contrast in the observations, causing the ocean temperature to have a smaller amplitude seasonal signal and lag continental temperatures in the march through the seasons. This effect is represented, albeit imperfectly, in the GCM. The land surface is in equilibrium with the solar insolation. The prescribed SSTs, however, are similar to the observed and reflect a lag between insolation and temperature. The perpetual season design of the model may tend to amplify the heat capacity effect because the system has essentially infinite time to adjust to this contrast.

Figure 4a is the modeled climatological precipitation, and Fig. 4b shows the JJA global precipitation distribution from Jaeger (1976). The zonal-mean rainfall maximum of the intertropical convergence zone (ITCZ) occurs in both (and in the DJF observations) at about 5° latitude in the summer hemisphere. The "lumpiness" of the ITCZ is more pronounced in the observations, with maxima reaching 10 mm day^{-1} where the maximum in the GCM climatology is 8 mm day^{-1}. Tropical precipitation maxima are associated with the Indonesian region as well as the African and American continents. Near subtropical Africa the observations and model show 2 mm day^{-1} precipitation. In the observations there is a monsoon precipitation maximum over equatorial Africa, but in the model

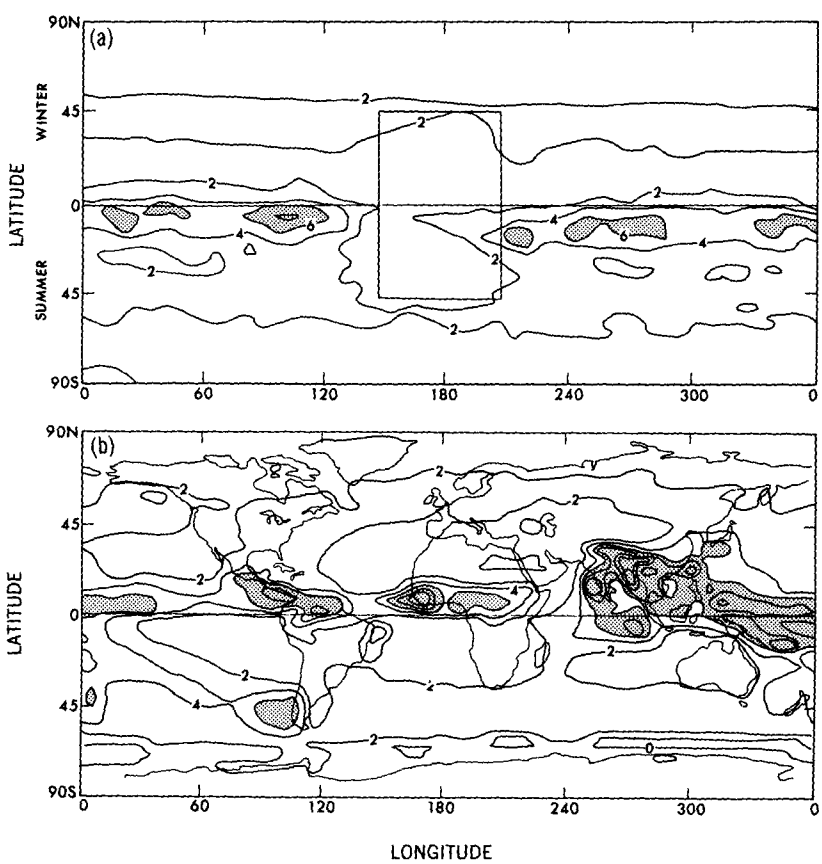

FIG. 4. Precipitation distribution for (a) GCM with hydrologically active (dry) continent and (b) observed JJA from Jaeger (1976). Contours are 2 mm day^{-1}.

there is a distinct break in the precipitation. Continental precipitation maxima are in the east in the model and in the west in the observations.

4. Continental climates

When the surface is allowed to participate in the hydrological cycle, very dry conditions prevail on the continent. Soil moisture values fall below 2 cm of water throughout the summer hemisphere and in much of the winter hemisphere. Figure 5 shows the soil moisture distribution on the continent in centimeters of water in the "bucket." The highest value possible of 15 cm is approached only in the poleward regions of the winter hemisphere. The only continential moisture occurs on the east coast of the summer subtropics.

We note in passing that this extreme soil moisture depletion was not expected. The result is independent of the initial conditions. This was tested by starting a hydrologically active continent experiment from the end of a saturated continent experiment, so that the atmosphere was already "spun up" when the surface hydrology was activated. With this experimental design, the atmosphere does not deplete the continental water to form the ITCZ, for example. In this case the continent dried out more slowly, but the equilibrium climatology was the same as in the experiment spun up from an isothermal atmosphere at rest.

Rather than being related to an intransitivity in the model climate, the extreme drying of the surface seems to be related to the perpetual season design of the experiment. An annual mean integration was performed in which the SST at a given latitude was equal to the average of the winter and summer values at that latitude from Fig. 1. In this case, the ITCZ is weakened over the continent but maintains over 3 mm day^{-1} of precipitation. Soil moisture values at the latitude of the ITCZ (the equator) are around 5 cm with drying below 2 cm only in the subtropics of both hemispheres. These results are not unlike earlier experiments with an annual mean sector model by Manabe (1969). Leaving the reasons for the extreme drying in our perpetual January experiment unexplored, at least for the present, we can consider that the experiment with an active surface hydrology is essentially equivalent to having prescribed a dry continent and explore the limits of climate processes in this extreme situation.

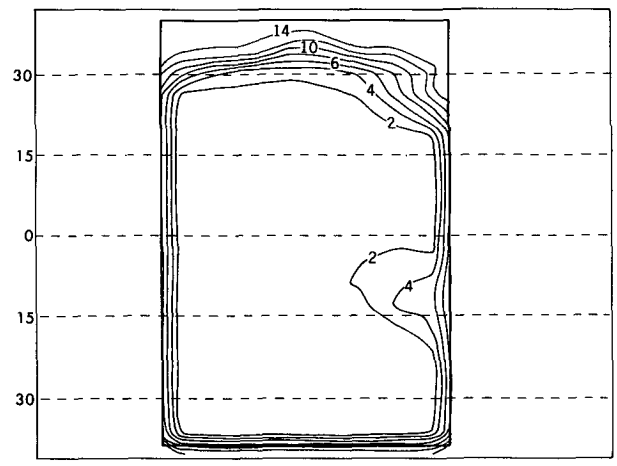

FIG. 5. Soil moisture from HYD. Contours are 2 cm of water.

Figures 6a and 6b are differences in the ground temperature (T^*) from the all-ocean control integration (the prescribed SSTs of Fig. 1). On the dry continent T^* is much warmer than on the saturated continent. The difference is zero away from the continent due to the fixed zonal-mean SST boundary conditions. On the saturated continent (Fig. 6a) the equator divides cooled and warmed land surfaces. In the summer hemisphere the warming reaches a maximum of 5 K near 30°, and there is little amplification of the warming in the continental interior. Cooling is largest over the snow-covered surface in the east where the midlatitude westerlies come onto the continent, as shown in the following section.

Over the dry continent (Fig. 6b) the substantially higher T^* differences, up to four times the values for the saturated continent, demonstrate the profound influence surface hydrology can have on a modeled continental climate. The T^* difference distribution is nearly identical to the distribution for the saturated continent poleward of 30° in the winter hemisphere, with cooling up to 8 K. (A third experiment identical to this one, but with no surface albedo changes due to snow, shows that the albedo change amplifies the winter hemisphere cooling by 2 K and has only local effects on the surface heat budget and the atmospheric dynamics.) Warming occurs throughout the summer hemisphere and also in the winter hemisphere from the equator to around 20°. In the winter hemisphere subtropics and in the summer hemisphere poleward of about 35°, the warming extends from coast to coast with slight amplification in the continential interior. There are two regions of maximum warming. A minor maximum occurs east of the center of the continent on the equator, where the temperature difference is nearly 12 K. In the summer hemisphere subtropics, a more distinct maximum extends across the continent with temperature differences up to 18 K. The smallest summer hemisphere temperature increases occur near 15° on the east coast.

Figure 7a shows the zonal mean values of the longwave, sensible, and latent heat fluxes from the surface to the atmosphere from the all-ocean control climatology. (The shortwave component is not shown since its influence is confined to the midlatitude snow field as discussed above.) The fluxes are generally larger in the winter hemisphere where the surface air is colder than the ocean and the winds are stronger. Throughout

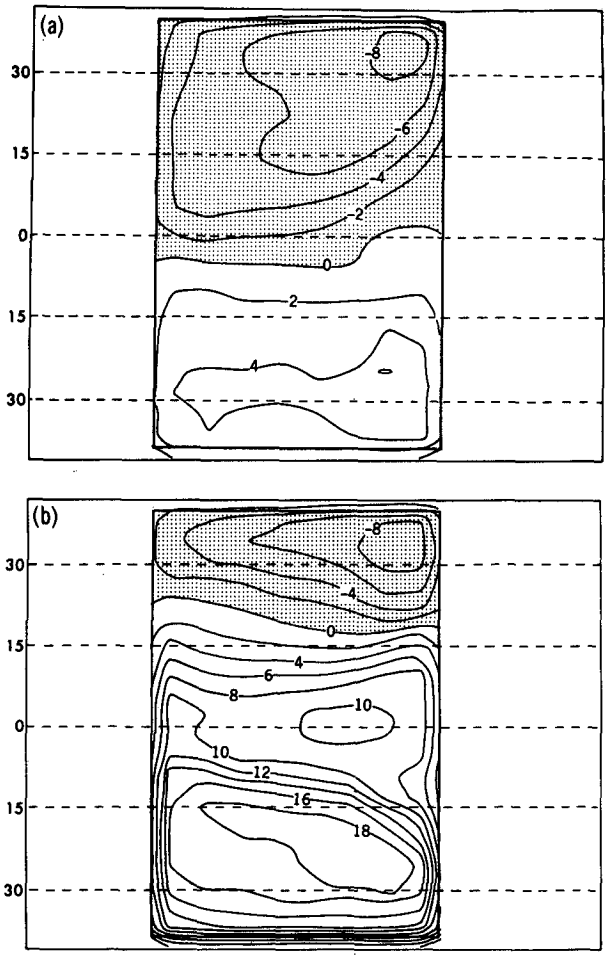

FIG. 6. Differences in the ground temperature between (a) the saturated continent and the control climate and (b) the dry continent and the control climate. Contour intervals are 2 K.

the tropics and subtropics (to 50° in the summer hemisphere and 30° in the winter hemisphere) the latent flux is the largest component of the surface heat balance, removing 70–140 W m^{-2} of heat from the surface to be deposited in the troposphere during condensation. The maximum at 10° latitude in the winter hemisphere corresponds to the maximum in the surface easterlies (Fig. 2a). The longwave flux has less pronounced latitudinal dependence and removes 50–70 W m^{-2} of heat from the tropical and subtropical ocean surface. Sensible heating accounts for about 20 W m^{-2} in these regions, dropping off quickly in middle latitudes like the latent component.

Figure 7b is the heat balance zonally averaged over land surfaces only in the saturated continent experiment. Both the latent and sensible fluxes are smaller than in the control in the winter hemisphere, and larger in the summer hemisphere. The latent contribution is the largest in the tropics and subtropics, as in the control, but the maximum has shifted to the summer hemisphere. The longwave flux from the saturated land surface is about 15 W m^{-2} larger at all latitudes than in the control. The magnitude of the sensible flux is similar to the control but the maximum is shifted from the winter hemisphere tropics.

Figure 7c shows how the components of the surface heat budget redistribute when the dominant surface cooling mechanism is disabled. Over the dry continent the latent heat flux is reduced to 60 W m^{-2} in the summer hemisphere tropics and less than 20 W m^{-2} in the winter tropics. This strongly resembles the zonal-mean precipitation distribution, suggesting that any rainfall immediately evaporates. Sensible and longwave cooling at the surface play approximately equal roles in the dry climate's heat balance. The longwave components again show less latitudinal dependence, removing 60–80 W m^{-2} throughout the tropics and subtropics, an increase of approximately 15 W m^{-2} as in the saturated continent case. The sensible component shows a larger response, with relative maximum (minimum) corresponding to relative minimum (maximum) in the latent heating, indicating compensation by the sensible flux for the decreased latent flux.

The distributions of the latent and sensible heat fluxes on the dry continent show that this compensation in the zonal-mean fields is not local. Figures 8a and 8b show differences (experiment minus control) in the latent and sensible heat fluxes. The latent heating minima near 10° in the winter hemisphere and 15° in the summer hemisphere are located in the west. The minima do not coincide with the temperature difference maxima, since their locations are also influenced by proximity to moisture sources and low-level winds to transport the moisture. The winter tropical minimum occurs in the west because the prevailing easteries bring moisture onto the east coast; the summer minimum is also associated with overlying dry continental air due to the induced cyclonic circulation (shown below).

The winter hemisphere sensible heating maximum (Fig. 8b) is located to the east of the latent heating minimum, reflecting the indifference of this field, at least indirectly, to the hydrological cycle. The summer hemisphere maximum is poleward and to the west of the T^* maximum due to influence from the low-level winds.

Precipitation differences from the all-ocean climatology for the saturated and dry continents are shown in Figs. 9a and 9b, respectively. Over the saturated surface precipitation increases by 1–3 mm day^{-1} across the entire breadth of the continent from 10° to 20° in the summer hemisphere, with decreases on the equator near the center of the continent and in the west. The net effect is a shifting of the ITCZ farther into the summer hemisphere in the western and central portions of the continent and a widening of the ITCZ in the east.

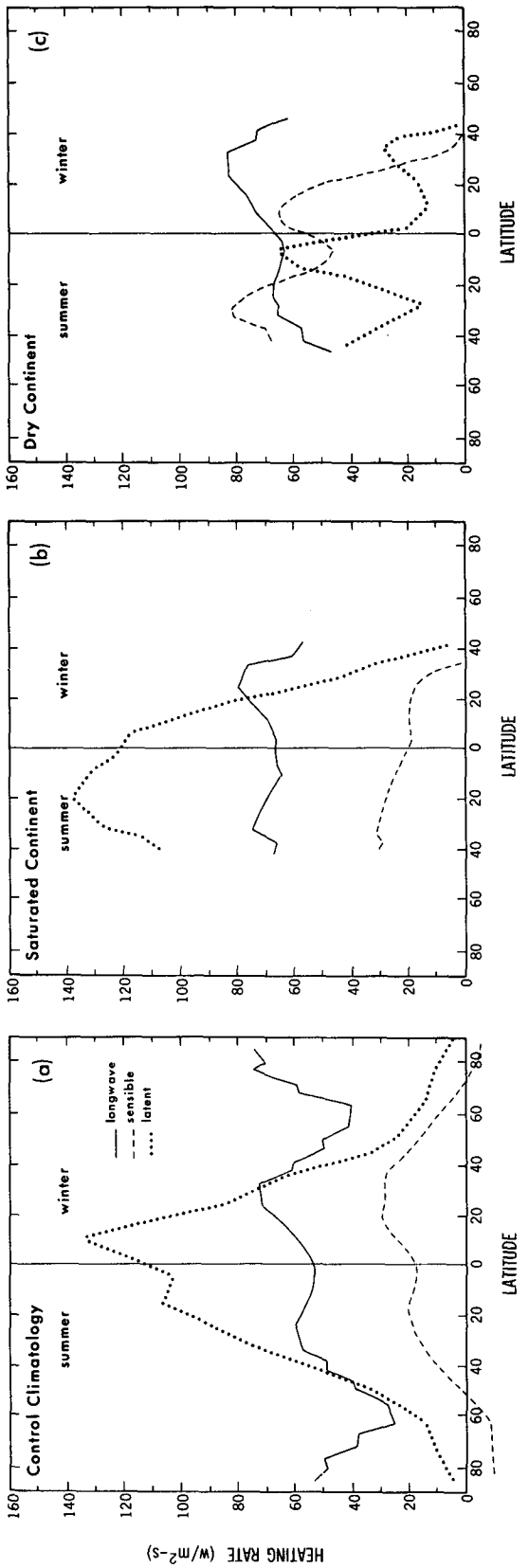

FIG. 7. (a) Zonally averaged components of the surface heat budget for the control climatology. Components of the surface heat budget over land only for the (b) saturated and (c) dry continent climatologies.

There are also two small regions where the precipitation seems to be larger off both coasts at about 10° in the summer hemisphere. There are no significant precipitation decreases in the summertime subtropics, but the winter hemisphere subtropical regions experience a decrease in the already minimal precipitation (see Fig. 4b).

The ITCZ is completely disrupted as it crosses the dry continent (Fig 9b). In contrast to the saturated case, precipitation decreases everywhere over the continent and even out over the oceans to the west at the latitude of the ITCZ. The winter hemisphere subtropical response is similar to the saturated case, with 1 mm day^{-1} decreases throughout the region. In the summer hemisphere subtropics precipitation decreases of up to 2 mm day^{-1} occur where there were no decreases over the saturated continent. One localized region of enhanced precipitation exists off the east coast in the summer hemisphere tropics as in the saturated case, but there is no sign of a maximum off the west coast.

With the documentation of the differences in the surface climate, we now ask how tropical circulation patterns differ over the wet and dry surfaces.

5. Tropical circulation

To explore the role of the tropical atmosphere in the climate's response to the continent, it is useful to consider two regimes in the troposphere. This division is motivated by differences in the atmospheric heating distributions and in the dynamical response to these fields.

The presence of the continent is communicated to the atmosphere through modifications of the heating fields. The horizontal distribution of the heating is affected, as well as where the heat is deposited in the vertical. Figures 10a and 10b are the total diabatic heating distributions at 515 mb in the saturated and dry continent experiments, respectively. The physical processes accounted for in the heating at the 515 mb level are radiative heating (shortwave and longwave), condensational heating due to predicted supersaturation, and adjustments due to excessive dry and moist adiabatic lapse rates. The heating distribution is very similar in the adjacent model layers at 350 and 680 mb in the dry continent case, and the pattern extends down to the 830 mb level as well over the saturated continent. Positive values of the summer hemisphere tropics are associated with latent heat releases, although it is not meaningful to distinguish between condensation performed due to supersaturated conditions and condensation that accompanies the moist adiabatic adjustment in the context of the model as discussed in the previous section. Longwave cooling causes the relatively small negative values at other latitudes. Details of the ITCZ structure in both experiments are clear,

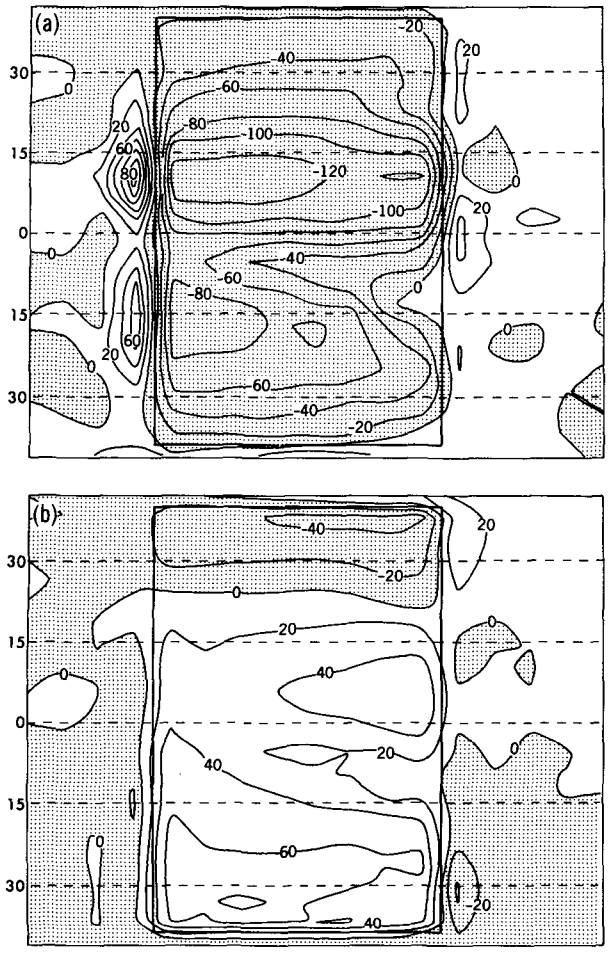

FIG. 8. Differences in the components of the surface heat balance for the dry continent minus the control: (a) latent cooling of the surface; (b) net upward sensible heat flux. Contour intervals are 20 W m^{-2}.

including the precipitation break over the dry continent shown in Fig. 4b where longwave cooling dominates the latent heating component.

The heating distribution is very different in the lower levels of the atmosphere. Figure 11a shows the net heating of the atmospheric layer at 940 mb for the saturated continent. The distribution is similar at 990 mb, with the warming at all latitudes equatorward of 60° in both hemispheres broken only by a region of weak cooling over the snow field associated with the reflection of solar radiation. The processes represented in this sum are the same as listed for the upper layer with the addition of vertical diffusion, which is accounted for only in the lowest four layers of the model. In the winter hemisphere, vertical diffusion is an important contributer to the total heating both over the continent and the oceans, with amplified fluxes over the continent. In the summer hemisphere the maxima on the subtropical continent are associated with dry convection (the dry adiabatic adjustment).

The magnitudes and horizontal gradients of the low-level heating are larger for the dry continent case shown in Fig. 11b. Radiative cooling rates decrease directly over the continent because low water vapor concentrations make the lower atmosphere more transparent to longwave radiation. The maximum in the winter hemisphere tropics is about equally associated with enhancements in the dry adiabatic adjustment and vertical diffusion. In the summer hemisphere the role of vertical diffusion is diminished and dry convection causes most of the layer heating.

The heating distribution in the lower layers is fundamentally different from that in the upper layers. The outline of the continent is clearly discernible in the low-level heating fields. Rather than being *perturbed* by the continent like the upper-level heating, the lower-level heating is *determined* by the continental conditions.

In the upper-tropical troposphere, vertical motion provides the primary dynamical response to the dia-

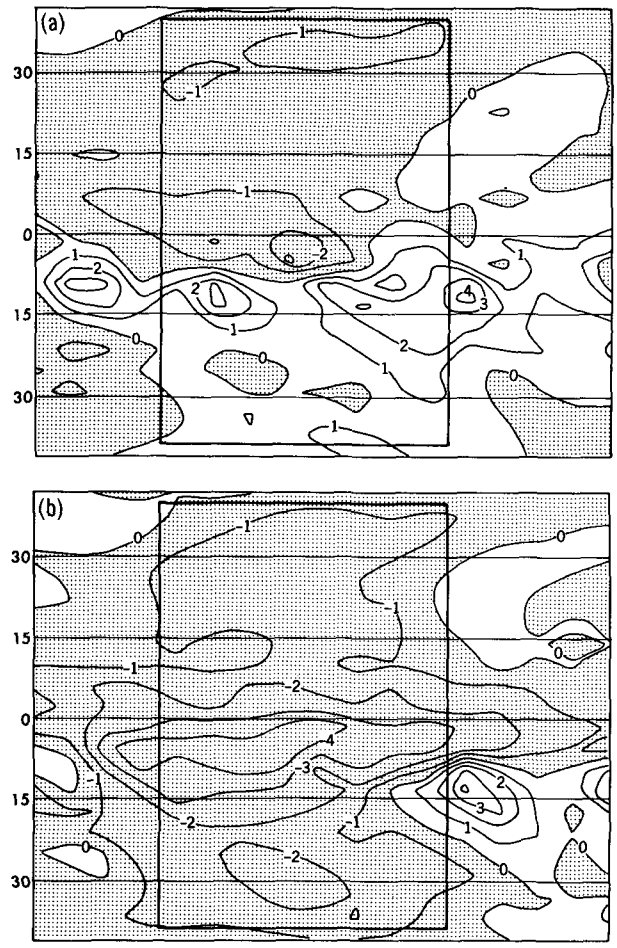

FIG. 9. Differences in precipitation between (a) the saturated continent and the control climate and (b) the dry continent and the control. Contours are 2 mm day^{-1}.

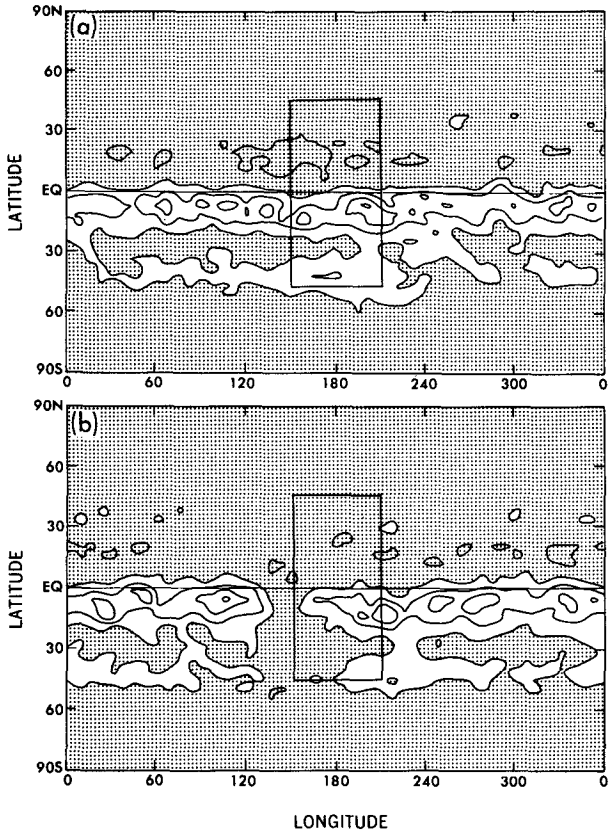

FIG. 10. Total diabatic heating rate at 515 mb for the (a) saturated continent and (b) dry continent. Contour intervals are 10^{-5} K s^{-1}, and regions of cooling are stippled.

batic heating. Adiabatic cooling and latent heating are highly correlated along the ITCZ in the model according to the simple thermodynamic equation

$$-S\omega = Q/c_p, \qquad (10)$$

where S is the static stability, ω is the vertical p-velocity, Q is the net diabatic heating rate, and c_p is the specific heat at constant pressure. Figures 12a and 12b show the adiabatic cooling ($-S\omega$) at 515 mb over the saturated and dry continents, respectively. (The climatological temperature is used to calculate S, and ω is also the time-mean value, so we are assuming that $\overline{S\omega} \approx \bar{S}\bar{\omega}$. This assumption is adequate for the idealized boundary conditions model with constant solar forcing, but may not be appropriate for a more realistic model.) The similarity to the net heating at the same level in the tropics (Figs. 10a and b) is striking from about 5° in the winter hemisphere to 25° in the summer hemisphere, with local latent heating maxima marked by strong negative p-velocities (upward motion). The interruption of the ITCZ over the continent is associated with reduced upward motion and even weak subsidence over the extreme western longitudes of the continent and out over the ocean where longwave cooling dominates. The connection between the heating and vertical velocity is less obvious at subtropical latitudes. The relationship represented by Eq. (10) does not exist at midlatitudes.

Heating in the lower layer drives a different, more complex, dynamical response. Figure 13a shows wind vectors on the 990 mb pressure surface from the saturated continent experiment, along with surface pressure isobars. The subtropical high is enhanced in the winter hemisphere subtropics over the continent. Wintertime midlatitude westerlies and tropical easterlies are perturbed, resulting in an anomalous anticyclonic circulation about the 1028 mb maximum. The surface pressure maximum is located under the downbranch of the strong wintertime Hadley circulation, equatorward of the maximum cooling shown in Fig. 6a. While the location of the Hadley cell is the same as that shown in Fig. 2b for the control climatology, mass transport by the direct cell over the land surface increases from about 160 to 220 $\times$ 10^9 kg s^{-1}.

The surface pressure minimum that develops over the saturated continent in the summer hemisphere is of comparable strength (4 mb) to the wintertime sub-

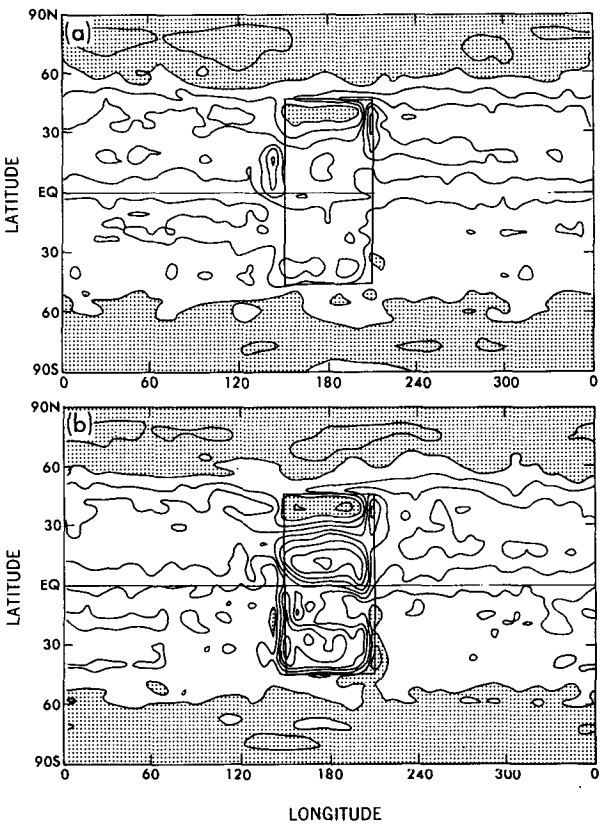

FIG. 11. Net diabatic heating at 940 mb for the (a) saturated continent and (b) dry continent climates. Contour intervals are 10^{-5} K s^{-1}, and regions of cooling are stippled.

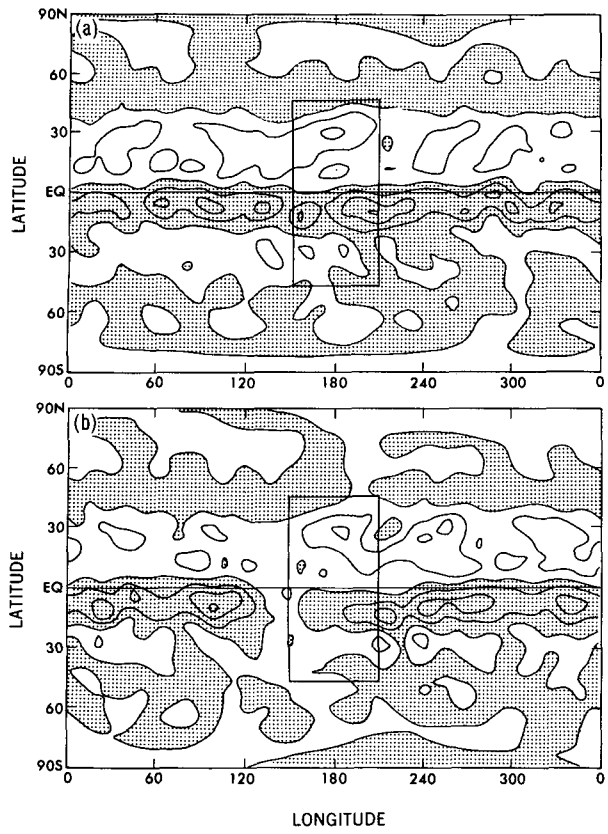

FIG. 12. Adiabatic cooling rate at 515 mb for the (a) saturated continent and (b) dry continent cases. Contour intervals are 10^{-5} K s^{-1}, and regions of cooling are stippled.

tropical high. It is located about 10° equatorward of the T^* difference maximum (see Fig. 6a) under the "upbranch" of the Hadley cell. As in the winter hemisphere, the Hadley circulation over land is enhanced, in this case to three times the strength of the cell over the ocean surface. The winter hemisphere tropical easterlies are drawn more across the equator, and northwesterly surface flow develops in the summertime tropics, contributing to weak cyclonic circulation about the pressure minimum. Flow parallel to the coast develops both in the east and west, and the tropical surface easterlies are decelerated out over the ocean to the east of the continent.

Figure 13b shows the surface pressure and wind vectors from the dry continent experiment. The modification of the pressure field and the associated low-level circulation in the winter hemisphere is similar to the saturated surface case. In the summer hemisphere, however, the low is more pronounced and positioned more centrally over the continent. Reference to Fig. 6b suggests that the location of the pressure minimum is more closely associated with the surface conditions (T^* difference distribution) than the large-scale circulation, and the low may be termed a "heat low." There is no surface pressure minimum associated with the T^* difference maximum on the equator. Cyclonic flow about the low is well developed over the dry continent. The perturbation of the wintertime tropical easterlies and midlatitude westerlies is stronger, as is the flow parallel to the east and west coasts. On the equatorial west coast, a monsoon flow onto the continent is induced as the tropical easterly flow is reversed and blows onto the continent from over the ocean.

In order to connect the differences in the circulation to differences in precipitation, consider where moisture convergence occurs in the model and what drives this convergence. In the control (and in the continent experiments away from the continents), a 15°-wide region of moisture convergence is centered under the ITCZ in the summer hemisphere. This moisture convergence zone is flanked by a zone of moisture divergence that extends from the equator to about 40° in the winter hemisphere, denoting the primary source of moisture for the ITCZ. In the summer subtropics zones of weak low-level moisture convergence alternate with regions of slightly stronger moisture divergence. Nearly all of the horizontal moisture convergence occurs below 680 mb.

Most of the column moisture convergence occurs below 680 mb over the continents also. Figure 14a shows the distribution of moisture convergence from the saturated continent experiment in the lowest three model layers. The quantity plotted is $\nabla \cdot (q\mathbf{v}_H)$, where q is mixing ratio and $\mathbf{v}_H$ is horizontal wind velocity on pressure surfaces, mass-integrated over the lowest three layers of the model (990, 940, and 830 mb). Regions of moisture convergence oriented perpendicular to the direction of the winter hemisphere easterlies alternate with regions of moisture divergence, but convergence dominates in the zonal mean. Two regions of moisture convergence are especially strong. One, over the western equatorial continent, extends out over the ocean with values above the noise within the ITCZ. This region is associated with the meeting of the weak monsoon circulation and the equatorward coastal flow (see Fig. 13a). A second region of anomalous moisture convergence occurs over the eastern half of the summer tropical continent. The long axis of this region lies parallel to the low-level winds that are drawn in from the winter tropical easterlies, and we can see the effect of these winds in pushing moisture convergence farther into the summer hemisphere. Moisture divergence occurs to the southwest parallel to the moisture convergence and can also be associated with the anomalous low-level flow toward the equator that is induced in the subtropics in response to the surface pressure heat low.

The low-level moisture convergence maxima are associated with precipitation maxima over the saturated continent. The double moisture convergence maximum in the west is directly under a similar structure

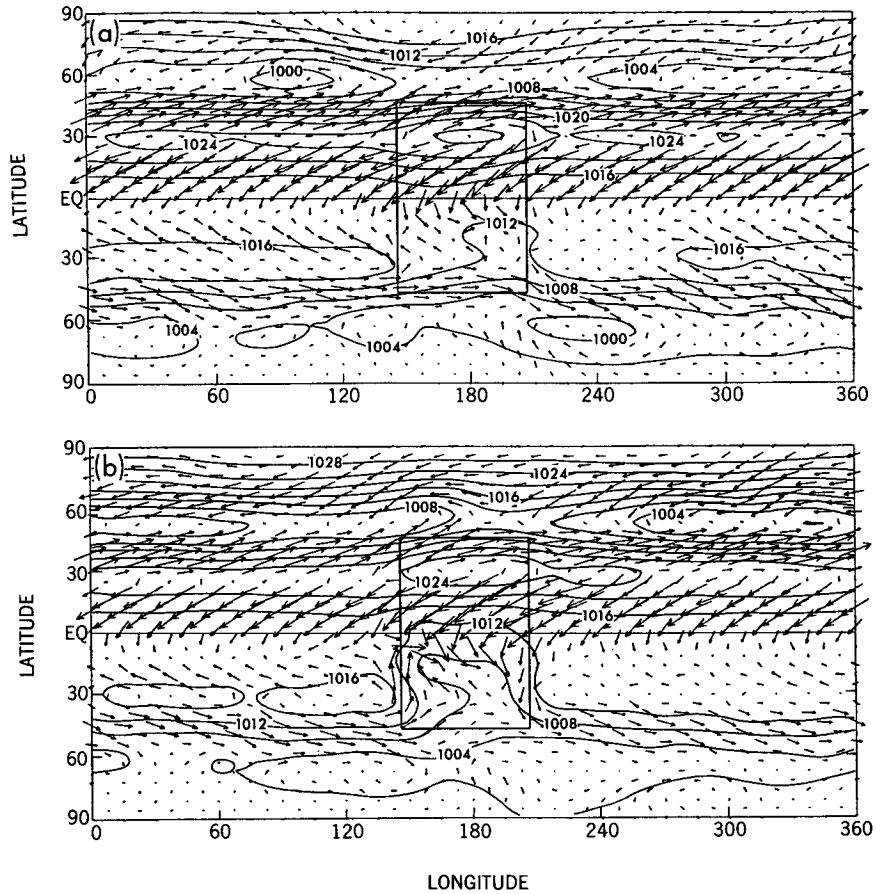

FIG. 13. Surface pressure and horizontal winds on the 990 mb pressure surface over the (a) saturated and (b) dry continents. Pressure contours are 2 mb, and the longest wind vectors are 6 m s^{-1}.

in the precipitation difference distribution (Fig. 9a). In the east, the moisture convergence maximum also lies under a similar precipitation feature, although the small precipitation difference maximum just off the east coast has no such analogy in the moisture convergence distribution. In general, however, a spatial connection between the low-level moisture convergence and condensation aloft is suggested. Given the connections between the moisture convergence and the low-level flow, we can conclude that the modifications of the precipitation over the saturated continent are determined by the response of the low-level winds to the warming of the continent and the attendant changes in pressure.

Figure 14b is the continent-induced moisture convergence over the dry continent. As in the previous case, moisture convergence and divergence are associated with the convergence and divergence of the low-level winds, but here sources of moisture also must be considered. The west coast moisture convergence between the equator and 15° in the summer hemisphere is larger and extends farther out over the ocean than in the saturated continent case. This can be related to the strong monsoon circulation and equatorward flow parallel to the coast driven by the large temperature differences at low levels in both hemispheres and the formation of the heat low in the summer hemisphere. Moisture convergence over the eastern half of the continent is less extensive over the dry surface because the winds blowing into this region have a continental origin. Although the diversion of the wintertime tropical easterlies into the summer hemisphere is more pronounced in this experiment, these winds also have a continental origin.

Moisture convergence distributions over both the dry and saturated land surfaces can be understood by considering the low-level flow in response to the surface heating and, in the case of the dry continent, sources of moisture at the surface. Unlike the saturated continent case, however, low-level horizontal moisture convergence is not a good diagnostic for precipitation, and we need to examine the vertical structure of the

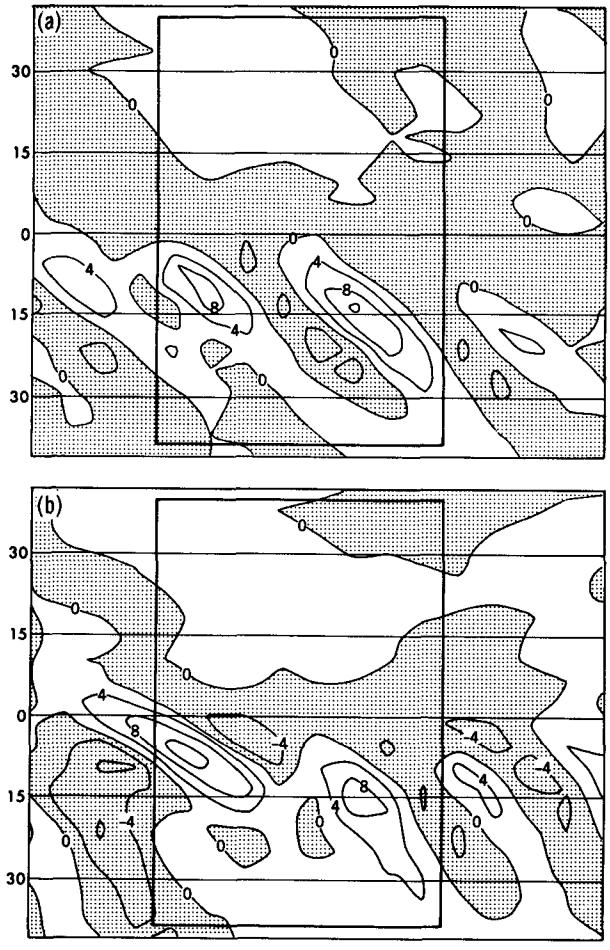

FIG. 14. Moisture convergence mass integrated over the lowest three model layers (990, 940, and 830 mb) for the (a) saturated and (b) dry continents. Shading indicates moisture divergence, with moisture convergence unshaded. Contour intervals are 2×10^{-7} s^{-1}.

circulation to understand the precipitation distribution. (This can also be the case in the subtropics, where low-level moisture convergence does not lead to condensation in the presence of large-scale subsidence associated with the down-branches of the Hadley circulation.)

In the control and saturated continent climatologies, vertical velocities increase upward through the 940 and, especially, 830 mb levels with little perturbation occurring over the saturated continent. In contrast, the vertical circulation and the mixing ratio are modified over the dry surface. Figure 15 shows (u, ω) vectors in a vertical cross section of the tropical troposphere at the latitude of the ITCZ (averaged over approximately 15° to 2° in the summer hemisphere) along with contours of water-vapor mixing ratio for the dry continent experiment. The depletion of water vapor below 830 mb is striking. Values are lowest over the western half of the continent where the very dry continental air reaches 800 mb. Above this level, mixing ratios are zonally uniform.

Vertical velocities are enhanced at low levels over most of the continent, with subsidence in the west. Strong vertical motion persists through 680 mb where the flow is divergent in this plane. At 515 and 680 mb vertical velocities are smaller than over the oceans, especially over the western half of the continent. This implies that less latent heating occurs to maintain the same mixing ratio values [cf. Eq. (10)].

Figure 16 shows the effects of condensation on the water-vapor mixing ratio. The quantity plotted is the climatological adjustment to the mixing ratio due to condensation associated with the moist adiabatic lapse rate adjustment and supersaturation alone as described in section 2. Over the ocean surface the largest values occur at the 940 mb level. From 680 to 350 mb values are fairly constant, with a weak maximum at 515 mb. Over the continent much of the condensation is eliminated below 680 mb. Even though the atmosphere experiences significant amounts of dry convection, mixing ratios are so low that the supersaturation criterion is difficult to meet. The temperature increase and mixing ratio decrease result in climatological relative humidities below 30% in the lowest layers, as opposed to over 80% over the ocean at the same latitude. In the midtroposphere, condensation persists over the eastern half of the continent but not in the west. With such a dry layer below, it is likely that including effects of reevaporation of falling raindrops would have an effect on soil moisture values in the east.

6. Conclusions

We have described experiments using a comprehensive, low-resolution (R15) GCM with idealized boundary conditions to investigate interactions between the tropical circulation and land surface conditions. The idealized boundary conditions involve zonally symmetrizing all external parameters, including insolation, SSTs, and clouds. Sea ice is not allowed to form, and the control integration includes no continental features. SSTs and solar forcing are prescribed to represent perpetual solstice conditions.

Two equilibrium experiments are conducted to compare with the control. Each is integrated for 700 days from isothermal, motionless initial conditions, with statistics taken from the last 500 days. In these experiments a large flat continent, 60° wide in longitude and extending to 45° latitude in each hemisphere, is imposed. In one experiment, the land surface is distinguished from the ocean surface only by its ability to change temperature in response to the surface heat balance; this continent is forced to remain saturated. In the second experiment, the continent is hydrologically active as well as able to change temperature. Soil moisture values, which are calculated using the

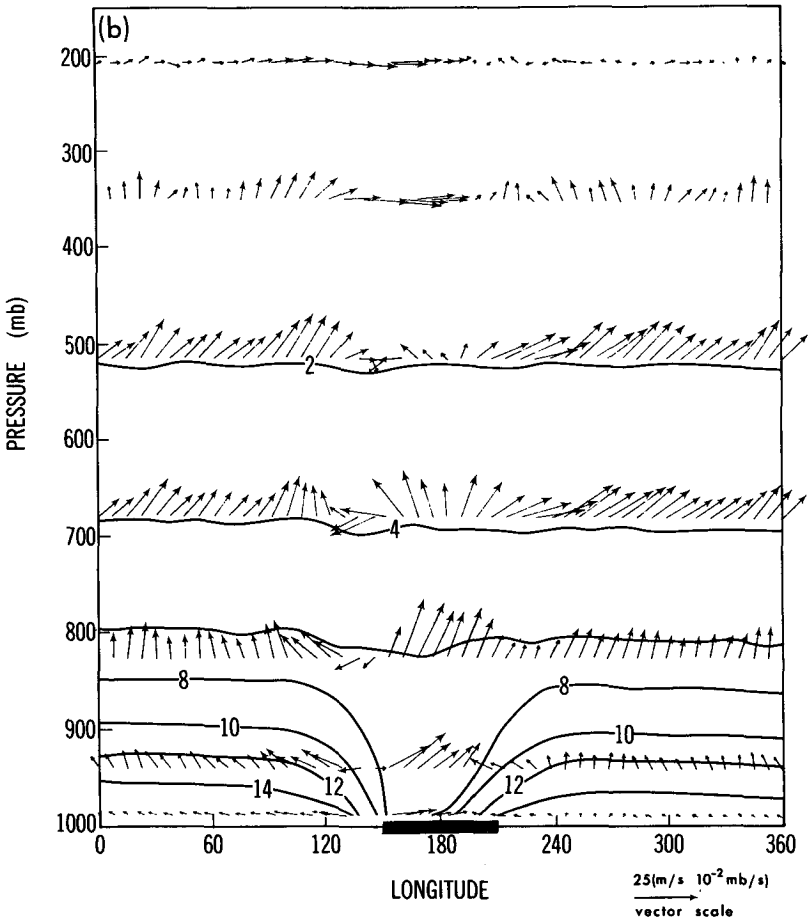

FIG. 15. Vertical cross section through the summer hemisphere tropics (15° to 2° latitude) of (u, ω) vectors along with lines of constant water-vapor mixing ratio for the dry continent experiment. Vector units are (m s^{-1}, 10^{-1} mb s^{-1}). Units of mixing ratio are grams per kilogram^{-1}.

"bucket" formulation, drop below 2 cm of water over most of the land surface.

The ground temperature on the saturated land surface warms by up to 4 K in the summer hemisphere and cools by up to 8 K in the winter hemisphere. Ground temperature increases are more than four times larger in the summer hemisphere in the arid continent case, and the warming spreads to 20° in the winter hemisphere. The ITCZ seems to shift farther into the summer hemisphere and become more coastal over the saturated continent, although the coarse resolution of the model does not allow a quantitative conclusion. There is also a decrease in precipitation in the already-dry winter hemisphere subtropics due to a strengthening of the Hadley circulation. The ITCZ is interrupted crossing the arid continent, and the subtropics in both hemispheres also experience a precipitation decrease. These results are similar to Druyan and Koster's (1989) experiments with a coarse-resolution GCM used to simulate a rainy and a drought Sahelian summer from different initial conditions. In the drought pattern, the ITCZ is broken in crossing Africa, and in the rainy simulation the ITCZ is continuous and shifted deeper into the summer hemisphere.

Over the tropical and subtropical ocean and saturated land surfaces in the model, the latent heating component of the surface heat budget is the largest, removing 80–135 W m^{-2} of heat. The longwave flux is about 60–70 W m^{-2} and the sensible component is about 20 W m^{-2}. Warming associated with the saturted continent causes the zonally averaged latent heating maximum to shift from the winter tropics, where the surface wind speed is the largest, to the summer tropics. The surface heat balance is altered over dry land, where the modeled latent heat flux ranges between 20 and 60 W m^{-2} throughout the tropics and subtropics. Small increases in the longwave and a tripling of the sensible fluxes compensate for the disabling of the latent flux. Maxima (minima) in the zonal-mean sensible flux are at the same latitudes as minima (maxima) in the zonal-

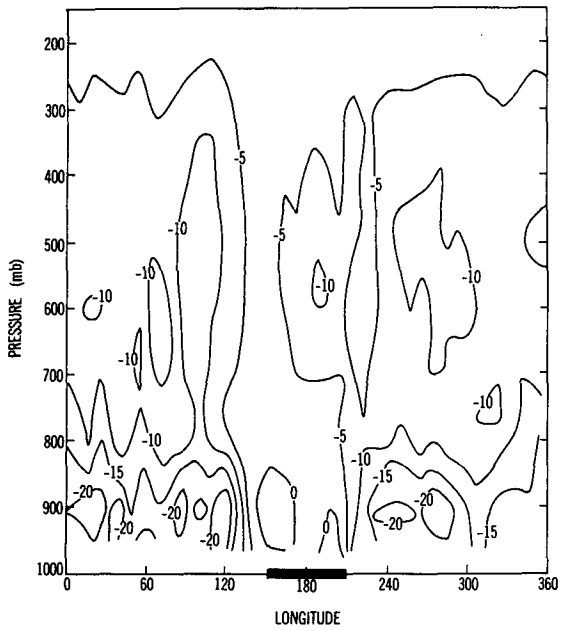

FIG. 16. Longitude-pressure cross section of the changes in water vapor mixing ratio due to condensation at the latitude of maximum precipitation (6.6 S) for the dry continent experiment. Contours are $5\ 10^{-7}\ s^{-1}$.

mean latent flux over land, but the "geographical" location of the sensible heating response is more sensitive to the ground temperature and surface wind response than the latent heating, which depends mainly on the hydrology in this case of extreme surface drying.

In the middle and upper tropical troposphere diabatic heating is mostly latent and is balanced by adiabatic cooling. The heating distribution, which is virtually identical to the ITCZ precipitation pattern, is interrupted over the dry continental surface. Below about 830 mb, the diabatic heating distribution is less zonal than in the upper layers, being dominated by the sensible heat flux from the land surface.

Over both the saturated and arid land surfaces, a thermal low and cyclonic circulation develop in the summer hemisphere subtropics. Tropical easterlies are accelerated and acquire a more pronounced cross-equatorial orientation in response to the surface pressure gradients. In the case of the saturated land surface, changes in precipitation are directly related to changes in low-level moisture convergence associated with the anomalous low-level flow. This results in the shifting of the ITCZ and its enhancement near both coasts.

Although low-level moisture convergence (and divergence) persists over the dry land surface in response to the strong heating gradients, it is unrelated to the modification of the tropical precipitation field. The lower atmosphere is very dry, with relative humidity below 30% in the lowest two layers of the model, so precipitation due to supersaturation is lost despite the decreased stability of the lower atmosphere. The effects of the dry continent reach into the midtroposphere, decreasing precipitation over the western half of the continent.

There is some relationship between the two extreme surface conditions studied here and observed connections between tropical circulation and precipitation patterns for Africa. Oceanic sources of moisture for Africa have been identified (e.g., Newell and Kidson 1979), but these are not necessarily well correlated with precipitation, with drought occurring even when the low-level moisture supply is maintained (Lamb 1983). In a classical desert circulation, the inability of the circulation to convert low-level moisture convergence into precipitation is associated with the large-scale subsidence of the down-branch of the Hadley circulation (Rasool 1984), and a strengthening of the mean meridional circulation has been connected with Sahelian drought (e.g., Nicholson 1981). Cadet and Nnoli (1987) also point out, however, the important role of evapotranspiration in the moisture budget for one summer over western Africa, this being central to concern that land use in a drought-sensitive area may tend to enhance the problem. Our study emphasizes the role of evapotranspiration over the continent in maintaining precipitation, supporting the idea that moisture convergence is not a sufficient condition for precipitation.

The physical processes associated with tropical "desertification" in this model would not be captured in a two-layer model because such a formulation cannot treat a decoupling of the upper and lower layers. A minimum of three layers would be needed to resolve the relevant structure. The simplest framework would include an upper layer in which adiabatic and diabatic heating balance, and a lower troposphere consisting of two layers so that changes in the vertical distribution of the moisture convergence and divergence patterns can develop in conjunction with surface drying.

A fundamental difference between tropical diabatic heating associated with SST anomalies and with continentality is highlighted. Without a drying of the surface, as in the control and saturated continent experiments, the dynamical response to heating is quite different from the case of the hydrologically active continental surface. Simple models that assume a balance between the latent heating and adiabatic cooling throughout the depth of the tropical tropopause omit the processes associated with tropical precipitation changes in these experiments.

These experiments describe the replacement of a tropical continental climate by an arid continental climate. The treatment is idealized and extreme, due in large part to the perpetual season formulation. The treatment of the surface hydrology is simple, clouds are not permitted to change, and factors related to surface albedo and roughness have not been considered.

The results can be used for guidance in examining the climates of more complex and higher-resolution GCM experiments, including realistic continents, higher horizontal resolution, seasonally and diurnally varying insolation, and, perhaps, interactive cloudiness.

Acknowledgments. KHC thanks Tom Delworth, Isaac Held, and an anonymous reviewer for their comments.

REFERENCES

Cadet, D., and N. Nnoli, 1987: Water vapour transport over Africa and the Atlantic Ocean during summer 1979. *Quart. J. Roy. Meteor. Soc.*, **113**, 581–602.

Delworth, T., and S. Manabe, 1988: The influence of potential evaporation on the variabilities of simulated soil wetness and climate. *J. Climate*, **1**, 527–547.

Dickinson, R. E. 1984: Modeling evapotranspiration for three-dimensional global climate models. *Climate Processes and Climate Sensitivity*, J. E. Hansen and T. Takahashi, Eds. *Geophys. Monogr.*, 29, Amer. Geophys. Union, 58–72.

——, 1986: Impact of human activities on climate—a framework. *Sustainable Development of the Biosphere*, W. C. Clark and R. E. Munn, Eds., Cambridge University Press, 252–288.

Druyan, L. M., and R. D. Koster, 1989: Sources of Sahel precipitation for simulated drought and rainy reasons. *J. Climate*, **2**, 1438–1446.

Jaeger, J., 1986: Monatskarten des Niedeschlags fur die Ganze Erde. *Ber. Dtsch. Wetterdienstes*, **139**, 38 pp.

Gill, A. E., 1980: Some simple solutions for heat-induced tropical circulation. *Quart. J. Roy. Meteor. Soc.*, **106**, 447–462.

Gordon, C. T., and W. F. Stern, 1980: A description of the GFDL global spectral model. *Mon. Wea. Rev.*, **110**, 625–644.

Lamb, P., 1983: West African water vapor variations between recent contrasting subSaharan rainy seasons. *Tellus*, **35A**, 198–212.

London, J., 1957: A study of atmospheric heat balance. Final Report. Contract AF19(122)–165, 62 pp. [Available from DDC College of Engineering, New York University.]

Manabe, S., 1969: Climate and the ocean circulation. The atmospheric circulation and the hydrology of the earth's surface. *Mon. Wea. Rev.*, **97**, 739–774.

Mintz, Y., 1984: The sensitivity of numerically simulated climates to land-surface boundary conditions. *The Global Climate*, John T. Houghton, Ed., Cambridge University Press, 79–105.

Newell, R. E., and I. W. Kidson, 1979: African mean wind changes between Sahelian wet and dry periods. *J. Climatol.*, **4**, 27–33.

——, J. W. Kidson, D. G. Vincent and G. J. Boer, 1972: *The General Circulation of the Tropical Atmosphere, Vol. 1*, The MIT Press, 258 pp.

Nicholson, S., 1981: Rainfall and atmospheric circulation during drought periods and wetter years in West Africa. *Mon. Wea. Rev.*, **209**, 2191–2208.

Rasool, S. I., 1984: On dynamics of deserts and climate. *The Global Climate*, J. T. Houghton, Ed., Cambridge University Press, 107–116.

Rind, D., 1982: The influence of ground moisture conditions in North America on summer climate as modeled in the GISS GCM. *Mon. Wea. Rev.*, **110**, 1487–1494.

Sellers, P. J., Y. Mintz, Y. C. Sud and A. Dalcher, 1986: A simple biospheric model (SiB) for use within general circulation models. *J. Atmos. Sci.*, **43**, 505–531.

Shukla, J., and Y. Mintz, 1982: The influence of land surface evaporation on the earth's climate. *Science*, **215**, 1498–1501.

Sud, Y. C., and M. J. Fennessey, 1984: Influence of evaporation in semi-arid regions on the July circulation: A numerical study. *J. Climate*, **4**, 383–398.

Walker, J., and P. R. Rowntree, 1977: The effect of soil moisture on circulation and rainfall in a tropical model. *Quart. J. Roy Meteor. Soc.*, **103**, 29–46.